Theoretical Studies of Au_m and $PtAu_n$ Clusters and Their N_2 and O_2 Adsorption Complexes

YA KUN CHEN,[1] WEI QUAN TIAN,[2] YAN ALEXANDER WANG[1]

[1]*Department of Chemistry, University of British Columbia, 2036 Main Mall, Vancouver, BC V6T 1Z1, Canada*
[2]*State Key Laboratory of Urban Water Resource and Environment, and Institute of Theoretical and Simulational Chemistry, Academy of Fundamental and Interdisciplinary Science, Harbin Institute of Technology, Harbin, Heilongjian 150080, China*

Received 22 March 2011; accepted 1 June 2011
Published online 7 December 2010 in Wiley Online Library (wileyonlinelibrary.com).
DOI 10.1002/qua.23200

ABSTRACT: Small homonuclear Au_m ($m \leq 5$) and bimetallic $PtAu_n$ ($n \leq 4$) clusters were studied using density functional theory. Both homonuclear and bimetallic clusters tend to form compact two-dimensional structures. All the low-lying Au_m clusters have delocalized highest occupied molecular orbitals (HOMOs), whereas all the $PtAu_n$ clusters have more localized HOMOs on the Pt atom. The localized HOMO makes the $PtAu_n$ clusters more regioselective toward electrophilic reactions than the Au_m clusters. Adsorptions of N_2 and O_2 onto these metal clusters were further studied. In N_2 adsorption, the metal clusters donate their electrons primarily to the σ^* orbitals of N_2 to form end-on complexes preferably. In O_2 adsorption, complicated π orbital interactions between the cluster and O_2 dominate to form side-on complexes with relatively larger binding energies.
 Int J Quantum Chem 112: 65–77, 2012

Key words: Au_m cluster; $PtAu_n$ cluster; N_2 adsorption; O_2 adsorption; bimetallic cluster

1. Introduction

With their special properties and reactivities, metal clusters have drawn a lot of attention in diverse research fields such as physics, chemistry, and materials sciences [1–6]. In comparison with their bulk counterparts, the unique size of small clusters contributes to their theoretical and practical importance. Because of their tunable electronic structure, bimetallic clusters are superior to homonuclear ones in many aspects. For example, bimetallic Ru–Pt clusters are good catalysts for hydrogenation of PhC_2Ph with enhanced or even unprecedented catalytic activities and selectivities [7]. Also, a series

Correspondence to: Y. A. Wang; e-mail: yawang@chem.ubc.ca
Contract grant sponsor: Natural Sciences and Engineer Research Council (NSERC) of Canada.
Contract grant sponsor: State Key Laboratory of Urban Water Resource and Environment at HIT (to W. Q. T.).

of bimetallic clusters containing many combinations of different transition metal elements have potential luminescence that can be used in photocatalysis at room temperature [8].

Particularly, Au and Pt, two third-row transition metal elements, have distinct properties and reactivities. Pt is chemically active and usually used as catalyst for various reactions. Au is often chemically inert and used as a coinage metal. Putting these two precious metal elements together, especially in small clusters, has resulted in many new advanced materials. For instance, CO adsorption on Pt can be enhanced by coating layers of Pt over a Au substrate [9]. Many experimental results suggest that bimetallic clusters of Au and Pt are better catalysts for many chemical reactions with much improved catalytic abilities than homonuclear Pt or Au clusters, because of the cooperative effect between Pt and Au. The silica-supported bimetallic Pt–Au clusters can activate absorbed CO by significantly lowering the stretching frequency of the C≡O bond (i.e., weakening the C≡O bond), whereas pure Pt catalysts do not have such potency [10]. Small Pt–Au bimetallic clusters also are recognized for their excellent performance in catalyzing the coupling reaction of CH_4 and NH_3 to produce the precursor for the important Degussa process [11–13].

Because traditional molecular spectroscopic techniques have intrinsic limits in characterizing these small clusters, theoretical calculations have become a powerful tool to gain deeper insights into the electronic structure of such clusters [14–17]. Recently, a series of density functional theory (DFT) calculations demonstrated that small Au clusters favor planar geometries, because the relativistic effect enhances s–d hybridization and d–d interaction [18, 19]. Some other DFT studies have suggested that small Pt clusters favor nonplanar geometries with high spin multiplicities [20–22]. It is then interesting to investigate the closely related Pt–Au bimetallic clusters for their geometric structures, catalytic activities and selectivities [23].

There are quite a few theoretical studies of adsorptions and reactions of small molecules (e.g., CO, O_2) on metal clusters, especially on Pt–Au bimetallic clusters [14–17]. Experimentally, the Pt–Au clusters were found to be good catalytic candidates to reduce various nitrogen oxide species in the presence of O_2 and small hydrocarbons [24, 25], in a desired, environmental friendly reaction route toward producing N_2 rather than other competing processes involving N_2O. O_2 concentration plays an important role in this better reaction path. Additional theoretical studies of the adsorption of N_2 and O_2 on the Pt–Au clusters can provide the necessary guidance in designing high-performance catalysts for the reduction of nitrogen oxide species. Besides this reaction, O_2 adsorption on metal clusters is also crucial for many other processes. For example, the cathode reaction of a fuel cell, typically the oxygen reduction reaction that throttles the fuel cell efficiency and performance, is greatly affected by the binding patterns of O_2 [26]. Without a doubt, N_2 and O_2 adsorption onto these clusters are of practical significance. Their adsorption complexes are investigated in this study.

Because of the large number of d electrons of the constituent atoms, calculations of the transition metal clusters have proven to be one of the most difficult tasks in quantum chemistry. DFT, combined with effective core potentials and their related basis sets, is a powerful, efficient tool to study such clusters, based on high-quality exchange-correlation functionals [27]. We thus adopted the Kohn-Sham DFT method in this study.

2. Computational Details

Full geometry optimizations of the metal clusters were carried out using the spin-unrestricted Kohn-Sham DFT method implemented in Gaussian03, with the PBEPBE exchange-correlation functional [28, 29]. Harmonic vibrational frequencies were computed to verify the nature of the stationary points on the potential energy surface. The double-zeta basis sets LanL2DZ and additional f-type polarization functions ($\alpha_f = 0.75$) for both Au and Pt atoms were used with the core electrons represented by the corresponding effective pseudopotentials [30]. An integration grid containing 99 radial shells and 590 angular points per shell was adopted to avoid spurious imaginary frequencies [31]. Electronic energies corrected for zero-point vibrational energy were used to establish the relative stability of metal cluster isomers. The standard Pople's 6-31G(d) basis set was used for nitrogen and oxygen. Partial charges and spin densities were calculated based on the natural bond orbital analysis [32].

To systematically sample the stationary points on the ground-state potential energy surface of the Au_m clusters, many topologically important structures were created as initial guesses. For the $PtAu_n$ clusters, the same sets of initial geometries were used with each nonequivalent Au position replaced by a Pt atom. Although many isomers were found for larger clusters, only the isomers lying

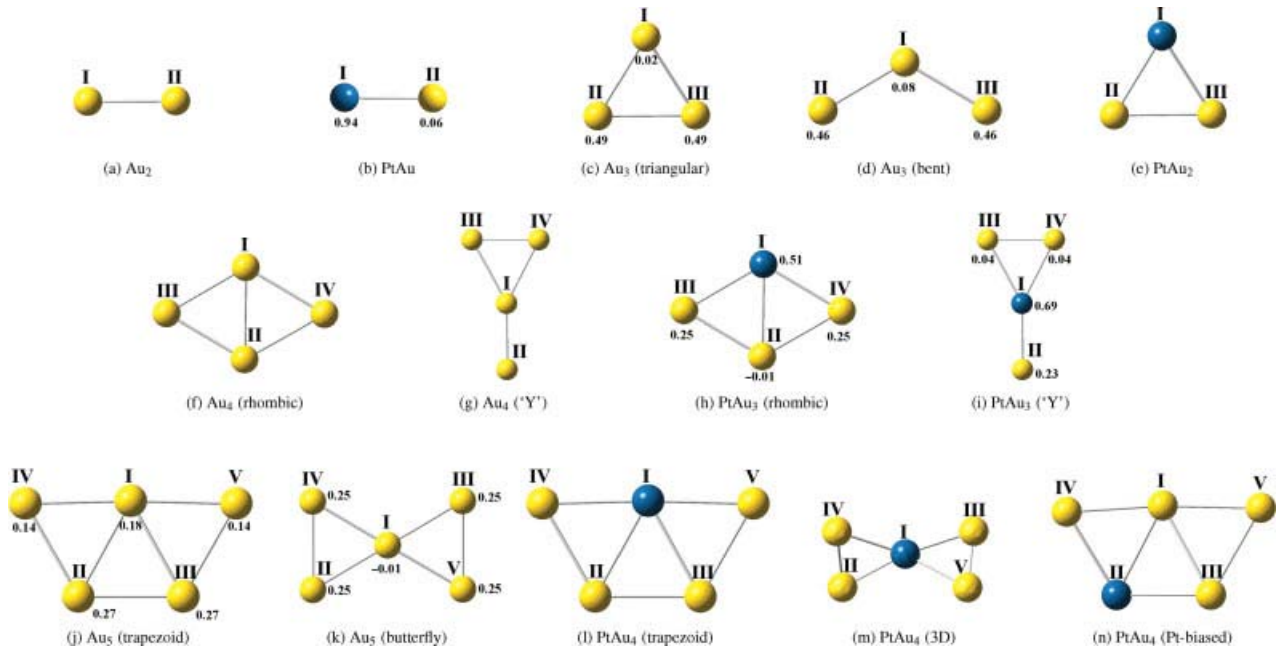

FIGURE 1. Optimized structures of low-lying Au_m and bimetallic $PtAu_n$ clusters. The Pt and Au atoms are in dark green and yellow, respectively. For open-shell clusters, natural spin charge on each atomic site is also shown. [Color figure can be viewed in the online issue, which is available at wileyonlinelibrary.com.]

within 10 kcal/mol of the ground-state structure were reported.

To study the adsorption complexes, we considered all clusters lying within 10 kcal/mol of the most stable isomer. N_2 and O_2 were placed at those topologically significant sites for subsequent geometry optimizations of the adsorption complexes.

3. Results and Discussions

3.1. Au_M AND $PtAu_N$ CLUSTERS

The structures of the most stable Au_m and $PtAu_n$ clusters and isomers (lying within 10 kcal/mol of the ground state) and the natural spin densities of the open-shell clusters are shown in Figure 1. The corresponding natural electronic configurations (NECs) are listed in Table I.

The predicted bond length and the frequency of the stretching mode of the ground-state Au_2 are 2.535 Å and 171.3 cm^{-1}, respectively, in good agreement with the experimentally observed values (2.473 Å and 190.9 cm^{-1}) [33, 34]. NEC analysis shows a slight electron promotion from 5d to 6s in both Au atoms and indicates the participation of the 5d orbital in the bond formation of Au_2.

As for the PtAu, the ground state has a $^2\Sigma^+$ electronic configuration. The bond length and fundamental vibrational frequency are 2.488 Å and 179.3 cm^{-1}, respectively, very close to the results obtained in some earlier high-level calculations using complete active space multiconfiguration self-consistent field method (2.601 Å and 168 cm^{-1}) and multireference singles and doubles configuration interaction method (2.544 Å and 194 cm^{-1}) [35]. The charge distribution of PtAu reflects the very small electronegativity difference between atomic Pt and atomic Au. In the PtAu cluster, only a small amount of negative charge is transferred from the Pt atom to the Au atom. The net spin charge is primarily localized on the Pt atom (see Fig. 1). NEC analysis indicates that the spin charge comes from the unfilled 5d orbital of the Pt atom, whose α-spin and β-spin valence NECs are $6s^{0.51}5d^{4.95}$ and $6s^{0.29}5d^{4.23}$, respectively.

Two low-lying Au_3 structures were identified (Fig. 1): an angular (bent) isomer with apex angle of 144.7°, and an isoceles triangular structure lying 1.73 kcal/mol above, with apex angle of 67.9°. In the angular Au_3, the Au(I)−Au(II)/Au(III) distance is 2.603 Å. In the triangular Au_3 isomer, the Au(I)−Au(II) and Au(II)−Au(III) distances are 2.630 and 2.936 Å, respectively. This indicates that

TABLE I

Natural electron configurations of atoms of the low-lying clusters.

Cluster	Atom	Sites	Natural electron configuration
Au_2	Au	I, II	[core]$6s^{1.05}5d^{9.94}6p^{0.01}$
PtAu	Pt	I	[core]$6s^{0.80}5d^{9.18}6p^{0.01}$
	Au	II	[core]$6s^{1.15}5d^{9.84}6p^{0.01}$
Au_3 (obtuse)	Au	I	[core]$6s^{1.19}5d^{9.83}6p^{0.03}6d^{0.01}$
	Au	II, III	[core]$6s^{1.04}5d^{9.92}6p^{0.01}$
Au_3 (acute)	Au	I	[core]$6s^{0.88}5d^{9.93}6p^{0.03}$
	Au	II, III	[core]$6s^{1.15}5d^{9.91}6p^{0.02}$
$PtAu_2$	Pt	I	[core]$6s^{0.69}5d^{9.47}6p^{0.02}$
	Au	II, III	[core]$6s^{0.97}5d^{9.92}6p^{0.02}$
Au_4 (rhombic)	Au	I, II	[core]$6s^{0.78}5d^{9.93}6p^{0.04}$
	Au	III, IV	[core]$6s^{1.35}5d^{9.88}6p^{0.01}$
Au_4 ('Y')	Au	I	[core]$6s^{1.17}5d^{9.83}6p^{0.04}$
	Au	II	[core]$6s^{1.26}5d^{9.89}$
	Au	III, IV	[core]$6s^{0.94}5d^{9.93}6p^{0.02}$
$PtAu_3$ (rhombic)	Pt	I	[core]$6s^{0.68}5d^{9.32}6p^{0.03}$
	Au	II	[core]$6s^{0.81}5d^{9.94}6p^{0.04}$
	Au	III, IV	[core]$6s^{1.20}5d^{9.86}6p^{0.02}$
$PtAu_3$ ('Y')	Pt	I	[core]$6s^{1.04}5d^{9.07}6p^{0.05}6d^{0.01}$
	Au	II	[core]$6s^{1.27}5d^{9.79}$
	Au	III, IV	[core]$6s^{0.97}5d^{9.90}6p^{0.02}$
Au_5 (trapezoid)	Au	I	[core]$6s^{0.97}5d^{9.87}6p^{0.06}$
	Au	II, III	[core]$6s^{1.03}5d^{9.91}6p^{0.03}$
	Au	IV, V	[core]$6s^{1.16}5d^{9.89}6p^{0.01}$
Au_5 (butterfly)	Au	I	[core]$6s^{1.02}5d^{9.85}6p^{0.07}$
	Au	II-V	[core]$6s^{1.08}5d^{9.91}6p^{0.02}$
$PtAu_4$ (trapezoid)	Pt	I	[core]$6s^{0.73}5d^{9.37}6p^{0.05}$
	Au	II, III	[core]$6s^{0.94}5d^{9.92}6p^{0.03}$
	Au	IV, V	[core]$6s^{1.13}5d^{9.88}6p^{0.01}$
$PtAu_4$ (3D)	Pt	I	[core]$6s^{0.96}5d^{9.33}6p^{0.06}6d^{0.01}$
	Au	II, III, IV, V	[core]$6s^{0.98}5d^{9.91}6p^{0.02}$
$PtAu_4$ (Pt-biased)	Au	I	[core]$6s^{0.88}5d^{9.89}6p^{0.05}$
	Pt	II	[core]$6s^{0.80}5d^{9.39}6p^{0.03}$
	Au	III	[core]$6s^{0.88}5d^{9.92}6p^{0.03}$
	Au	IV	[core]$6s^{0.80}5d^{9.39}6p^{0.03}$
	Au	V	[core]$6s^{1.25}5d^{9.89}6p^{0.01}$

The atomic sites are shown in Figure 1.

the Au(I)−Au(II)/Au(III) interaction in the angular isomer is stronger than that in the triangular one. Most of the spin density is evenly located on the two equivalent Au atoms in both Au_3 isomers. According to the NEC analysis, the middle Au atom in the angular Au_3 undergoes electron promotion from 5d to 6s and electrons migrate from the two terminal Au atoms to the central one. In contrast, in the triangular Au_3, the apex Au atom donates its electrons to the basal Au atoms. The most stable $PtAu_2$ is also an isoceles triangular cluster with the apex angle of 67.7° and the Pt–Au bond length of 2.579 Å. Electrons flow from the 5d and 6s orbitals of two basal Au atoms to the 5d orbital of the apex Pt atom.

As to the clusters larger than the trimer, the low-lying Au_m and $PtAu_n$ clusters are constituted of colaterally packed triangular building blocks to form (near) two-dimensional structures. In the low-lying $PtAu_n$ clusters, the Pt atom tends to maximize its coordination number to stabilize the cluster by forming a maximal number of bonds with the surrounding atoms.

In the case of the Au_4 clusters, the ground state is a singlet planar rhombic structure, which is essentially

degenerate with a singlet Y-shaped structure found in an earlier study [36]. The $PtAu_3$ has a $^2A''$ ground state with a puckered rhombic configuration and a folding angle of 27.2°. An essentially degenerate $^2A'$ Y-shaped isomer lies 0.97 kcal/mol above the ground state of $PtAu_3$ with the Pt atom at the center. In the rhombic Au_4 and $PtAu_3$ clusters, the atoms at positions I and II donate their electrons to the 6s orbital of the Au atoms at sites III and IV. In the Y-shaped Au_4 and $PtAu_3$ clusters, the Au atoms at positions III and IV donate their electrons to the apex atom. Spin densities in the two $PtAu_3$ clusters are mainly located on the Pt atom.

The most stable isomer of Au_5 is a $^2A'$ planar trapezoid-like structure, as reported earlier [36]. A $^2B_{2u}$ butterfly-like configuration lies 8.15 kcal/mol above the most stable trapezoid isomer. In both these two low-lying Au_5 clusters, all the Au atoms undergo electron promotion from 5d to 6s to form Au−Au bonds and Au at site I contributes electrons to the other four Au atoms. The most stable isomer of $PtAu_4$ is also a planar trapezoid-like structure with the Pt atom lying at the middle of the long parallel side to maximize its coordination number. A three-dimensional isomer with a twisted butterfly-like geometry lies 2.39 kcal/mol above the trapezoidal $PtAu_4$. Another $PtAu_4$ (Pt-biased) isomer is 8.62 kcal/mol higher than the trapezoidal structure. The substitution of Au by a Pt atom at site II in the trapezoidal Au_5 cluster distorts the cluster to a nonplanar structure. In all these three $PtAu_4$ isomers, electron transfer from 6s to 5d occurs to the Pt atom and the Pt atom withdraws electrons from the other Au atoms, yielding a negative partial charge.

To gauge the reactivity of these clusters, their Kohn-Sham frontier molecular orbitals and the orbital energies of these clusters are shown in Figure 2. The highest occupied molecular orbital (HOMO) of Au_2 is a σ orbital and the lowest unoccupied molecular orbital (LUMO) is a σ^* orbital. The large HOMO−LUMO gap and the low HOMO energy (−6.6 eV) make the Au_2 cluster inert to electrophilic attack. In PtAu, the HOMO is mainly the 5d orbital of the Pt atom and has a much better donating ability with an increased orbital energy (−5.9 eV). The LUMO is again a σ^* orbital with a similar orbital energy to the LUMO of Au_2. For most larger clusters, the HOMOs of the $PtAu_n$ clusters are mainly composed of the 5d orbitals of the Pt atom and have orbital energies close to −5.3 eV. The HOMOs of the Au_m clusters are delocalized over the entire cluster and have orbital energy lower than −5.3 eV. The LUMOs of the $PtAu_n$ and Au_m clusters are typically σ^* orbitals and have similar orbital energies of about −4.5 eV. Therefore, the attacking electrophiles will readily locate the reactive Pt center of the bimetallic clusters because the Pt atom of the bimetallic clusters accumulates more negative charge than the Au atom of the corresponding pure Au_m clusters of the same size at the same position.

3.2. ADSORPTIONS OF N_2 AND O_2

With the optimized low-lying clusters in hand, the complexes formed by adsorbing N_2 and O_2 onto these low-lying clusters were studied. Thirty three N_2–cluster and 48 O_2–cluster complexes were obtained from geometry optimization. The Hessians of these optimized structures were calculated to verify the nature of these complexes. Figures 3 and 4 show the structures of energetic minima. The adsorption energies are shown in the two figures. Negative adsorption energies denote exothermic adsorption. Within the same chemical composition, the energy of the most stable isomer was taken to be the reference point in calculating the relative energies of all possible complexes. The N–N and O–O bond lengths are listed to illustrate the interaction strengths between the diatomic molecules and the metal clusters.

In all adsorption complexes, to stabilize the complexes through enhanced electrostatic interaction, the metal clusters donate electrons to the O_2/N_2 diatomic molecular fragments based on the charge analysis (see below). Almost always, the binding energies of O_2/N_2–bimetallic cluster complexes are larger than that of the complexes formed between N_2/O_2 and the corresponding pure Au clusters of the same size. Binding N_2/O_2 to the Pt atom of the bimetallic clusters typically has an adsorption energy of about 30 kcal/mol, larger than that to the pure Au clusters (20 kcal/mol). For the binary $PtAu_n$ clusters, the high adsorption energy correlates specifically to the binding of O_2 or N_2 to the Pt atom rather than to the Au atoms, because the HOMO is mainly localized on the Pt atom in the bimetallic clusters. The adsorption complexes formed by pure Au clusters are similar to the complexes formed by the small diatomic molecules and the bimetallic clusters on the Au site. Therefore, the complexes involving pure Au clusters are not discussed specifically.

Geometrically, both O_2 and N_2 prefer to bind to the clusters to the side within the plane of the cluster. Even though the major lobe of the HOMOs of these clusters are atop the clusters, the side-on binding enables the clusters to donate electrons to form

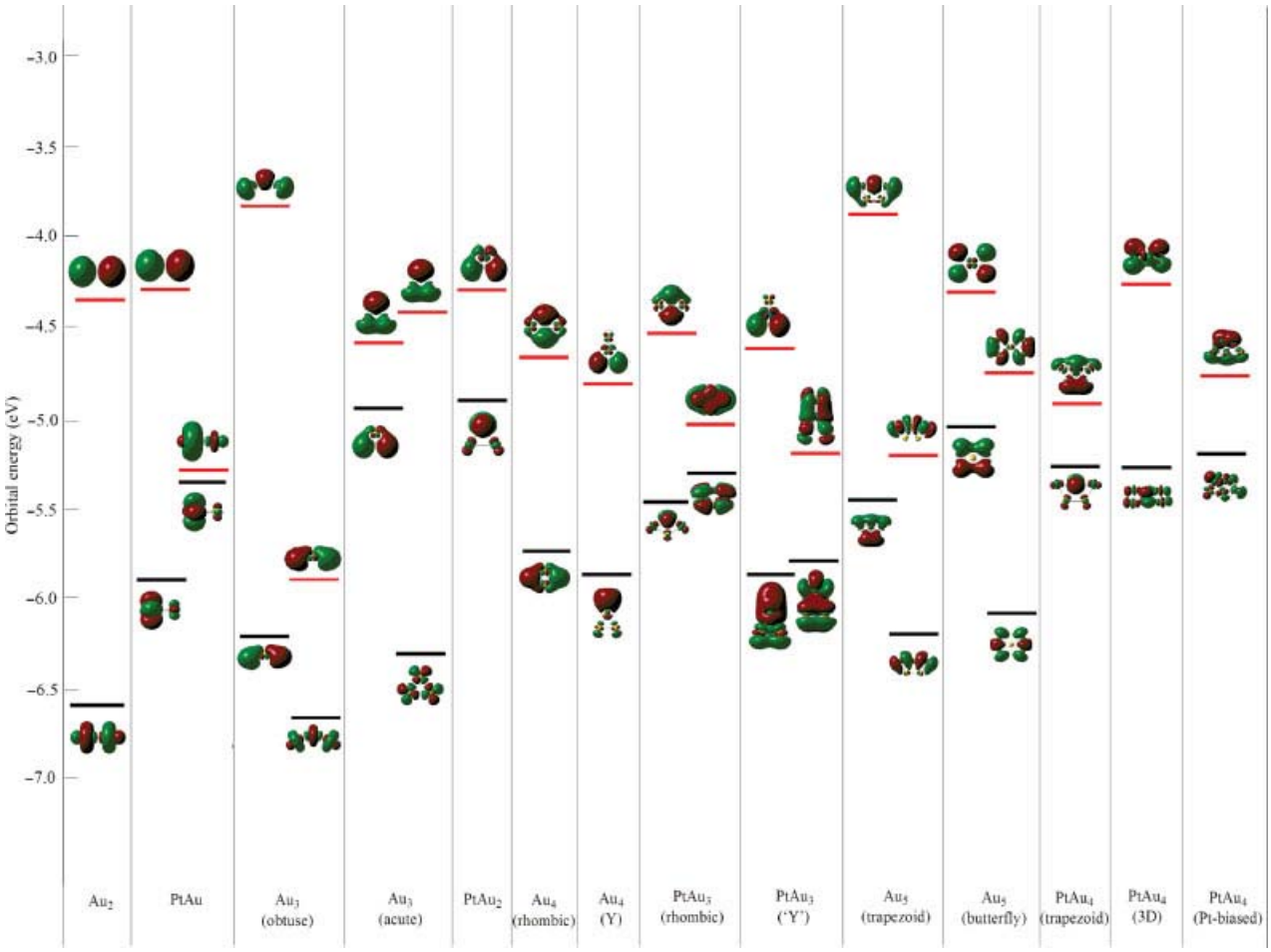

FIGURE 2. The frontier molecular orbitals of Au_m and $PtAu_n$ clusters. The orbital energies of the highest occupied molecular orbitals and the lowest unoccupied molecular orbitals are marked by black and red bars, respectively. For open-shell systems, α-spin and β-spin orbitals are grouped on the left and the right of each column, respectively. [Color figure can be viewed in the online issue, which is available at wileyonlinelibrary.com.]

both σ and π bonds. In contrast, if the diatomic molecule binds to the cluster top, only a σ bond will be formed instead.

Besides the difference in binding strength, N_2–adsorption complexes also distinguish themselves from the O_2–adsorption complexes in many aspects that will be discussed below based on the representative O_2/N_2-PtAu_2 complexes. As the precursor $PtAu_2$ cluster donates electrons to either N_2 or O_2 fragments on the formation of complexes, the HOMO of the $PtAu_2$ cluster must play an important role. The HOMO of $PtAu_2$ mainly locates on the Pt atom and is composed of the 5d orbital of the Pt atom (17% $5d_{z^2}$, 57% $5d_{x^2-y^2}$, and 3% 6s) with some minor contributions from the two basal Au atoms (ca. 4% from their 5d orbitals). This particular composition of the HOMO makes the absorbate diatomic molecules preferentially attach to the Pt atom.

To have an overall view of the electronic structures of N_2/O_2–$PtAu_2$ adsorption complexes, the total density of states (DOS) and the local DOS (LDOS) for selected complexes ($PtAu_2N_2^{A,B,C}$ and $PtAu_2O_2^{A,B,C}$) and the precursor $PtAu_2$ are shown in Figures 5. The DOS in the valence region (−10 eV below the Fermi level) of these complexes can be divided into three domains according to the source of their origins. In domain I (from −7.0 eV to the Fermi level), the LDOS of the Pt atom dominates the total DOS. In domain II (from −11.0 to −7.0 eV), the total DOS is mainly composed of the LDOS of the Au atoms. In domain III (below −11.0 eV), the LDOS of the diatomic absorbates have the most contribution. In $PtAu_2N_2^{A,B}$, adsorption of N_2 on the Pt atom of the clusters shifts

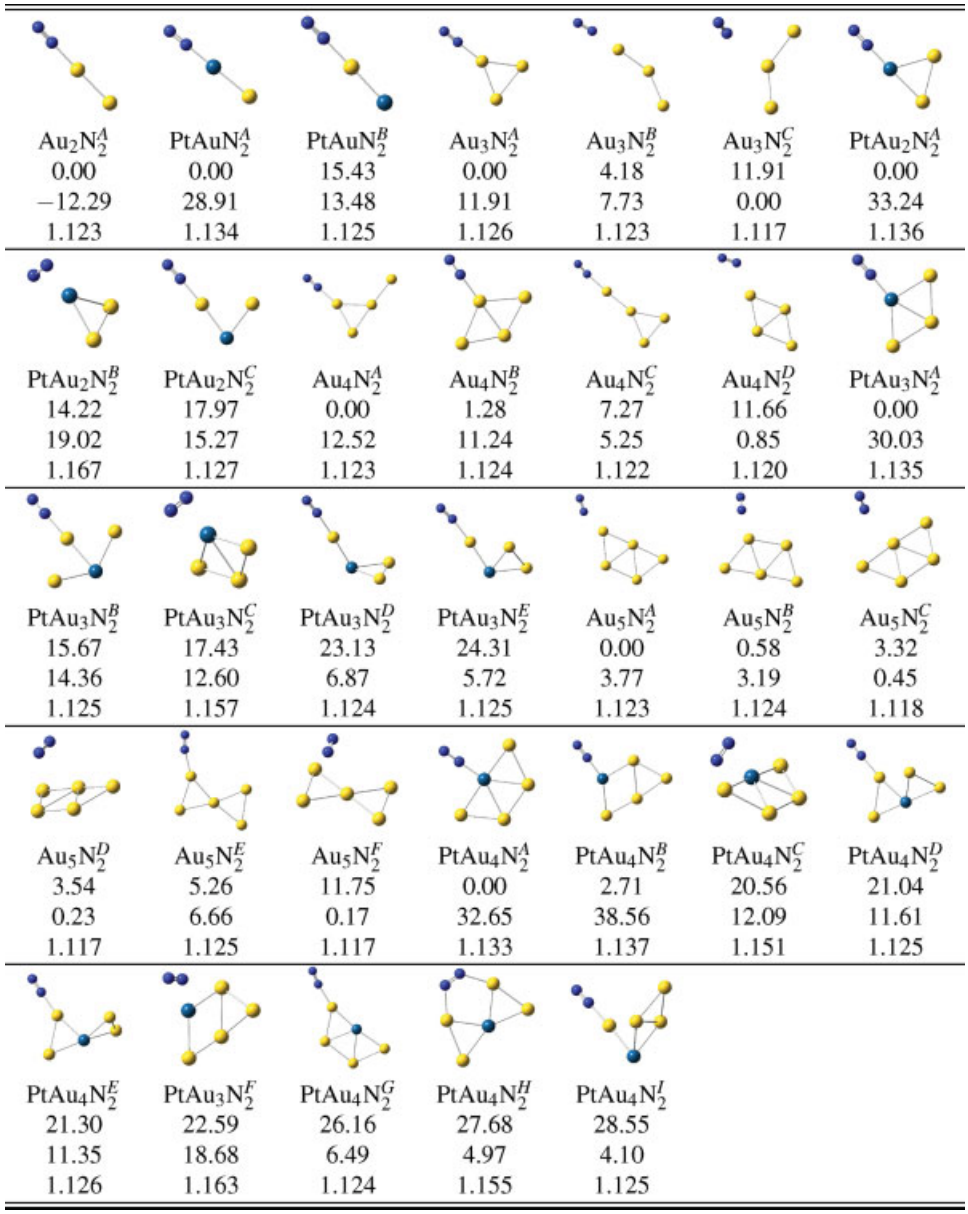

FIGURE 3. The optimized structures of N_2–cluster adsorption complexes. The relative energy (in kcal/mol) measured from the most stable complex, the adsorption energy (in kcal/mol), and the N−N bond length (in Å) are listed below each optimized structure descendingly. [Color figure can be viewed in the online issue, which is available at wileyonlinelibrary.com.]

the electronic states of the pure bimetallic cluster $PtAu_2$ in domain I to a lower energy level but keeps domain II almost intact. In the case of O_2 adsorption, the total DOS in both domains I and II moves to lower energy levels regardless of the O_2 adsorption site on the cluster. It is clear that the adsorption of N_2 onto the clusters locally perturbs the electronic structure of the cluster fragment around the adsorption site, whereas O_2 adsorption modulates the LDOS of the cluster to such a large extent that the LDOS of those atoms not directly bound to the O atoms are also influenced. For the complexes with the side-on adsorption pattern ($PtAu_2N_2^B$ and $PtAu_2O_2^{A,B,C}$), their DOS are characterized by many peaks between −15.0 and −11.0 eV, which arise from the versatile bonding interactions between the absorbates and the clusters. The π orbitals in the plane of the diatomic adsorbate molecule and the Pt atom of the bimetallic

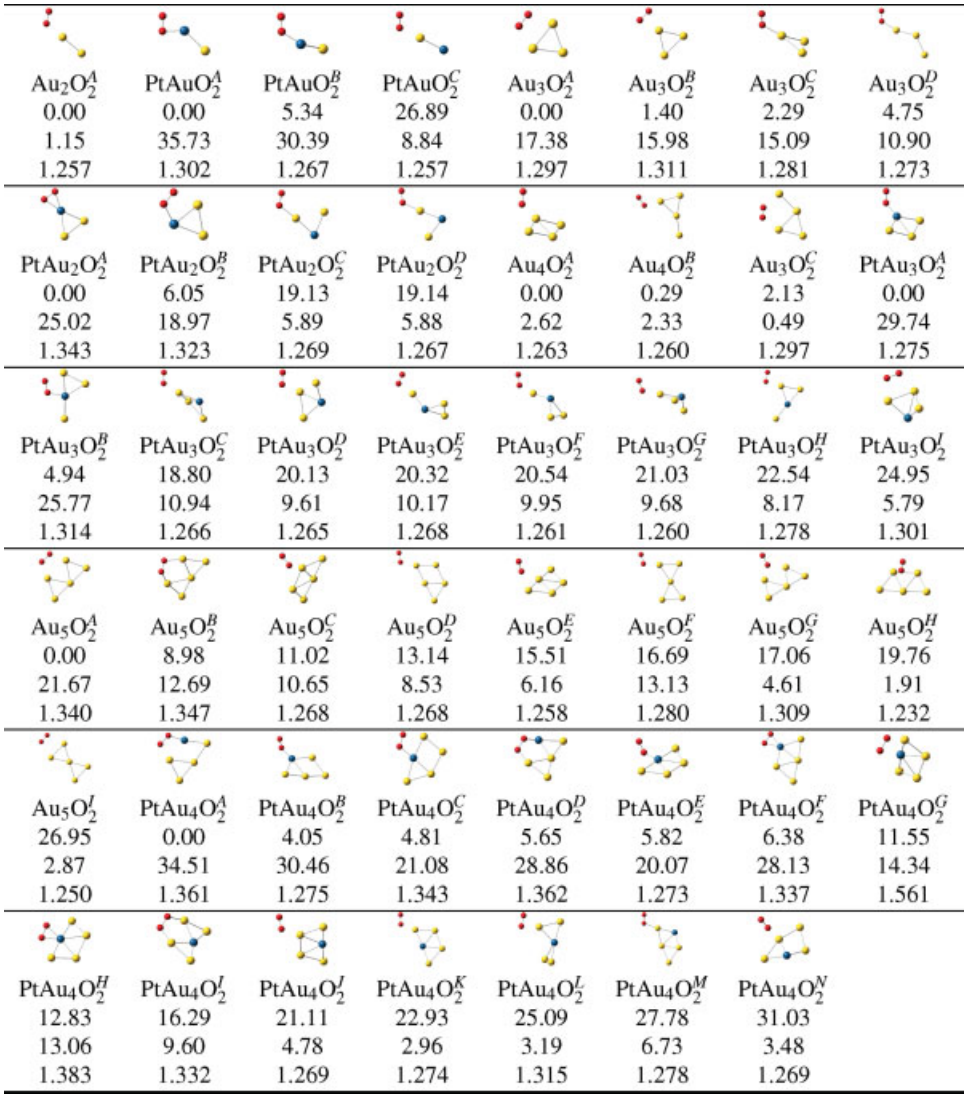

FIGURE 4. The optimized structures of O_2–cluster adsorption complexes. The relative energy (in kcal/mol) measured from the most stable complex, the adsorption energy (in kcal/mol), and the O–O bond length (in Å) are listed below each optimized structure descendingly. [Color figure can be viewed in the online issue, which is available at wileyonlinelibrary.com.]

cluster can have σ-type interactions, while the π orbitals perpendicular to this plane can engage in π-type interactions. In contrast, the end-on binding complexes have a few sparsely distributed states in the same energy range, indicating relatively simple bonding interactions between the cluster and the absorbate. The detailed bonding interactions are further discussed for N_2– and O_2–adsorption complexes in the following section.

3.3. N_2 AND O_2 ADDUCTS

In most cases, N_2 tends to bind to the clusters in an end-on fashion, except for the bimetallic $PtAu_2N_2^B$, $PtAu_3N_2^C$, and $PtAu_4N_2^C$ complexes. To understand the interaction between N_2 and the bimetallic clusters, molecular orbitals relevant to the bonding interactions in the above three N_2-PtAu_2 complexes are shown in Figure 6. Both σ and π orbitals contribute to the bonding interactions in the $PtAu_2N_2^A$ complex and a similar set of bonding orbitals can also be found in the $PtAu_2N_2^C$ complex. The σ bonds (e.g., HOMO-16 and HOMO-19) that hold the absorbate and the cluster come from the overlap between the σ type orbital of N_2 and the Pt 6s5d orbitals. The two π-type bonds (e.g., HOMO-17 and HOMO-18) result from the overlap between the two perpendicular π

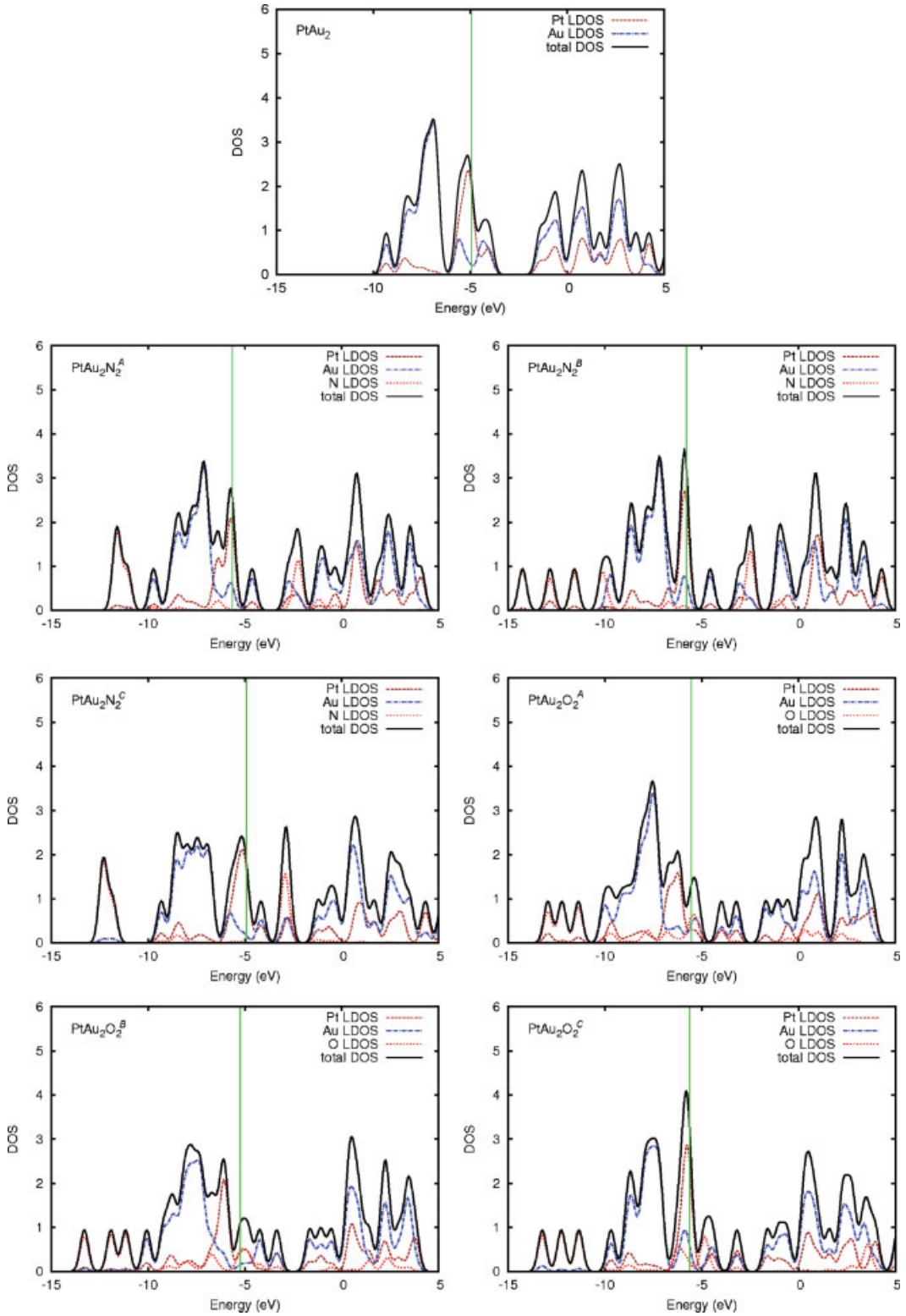

FIGURE 5. The total density of states (DOS) and local DOS (LDOS) projected onto each element of the $PtAu_2-N_2$ and $PtAu_2-O_2$ adducts. Green vertical lines mark the Fermi levels. [Color figure can be viewed in the online issue, which is available at wileyonlinelibrary.com.]

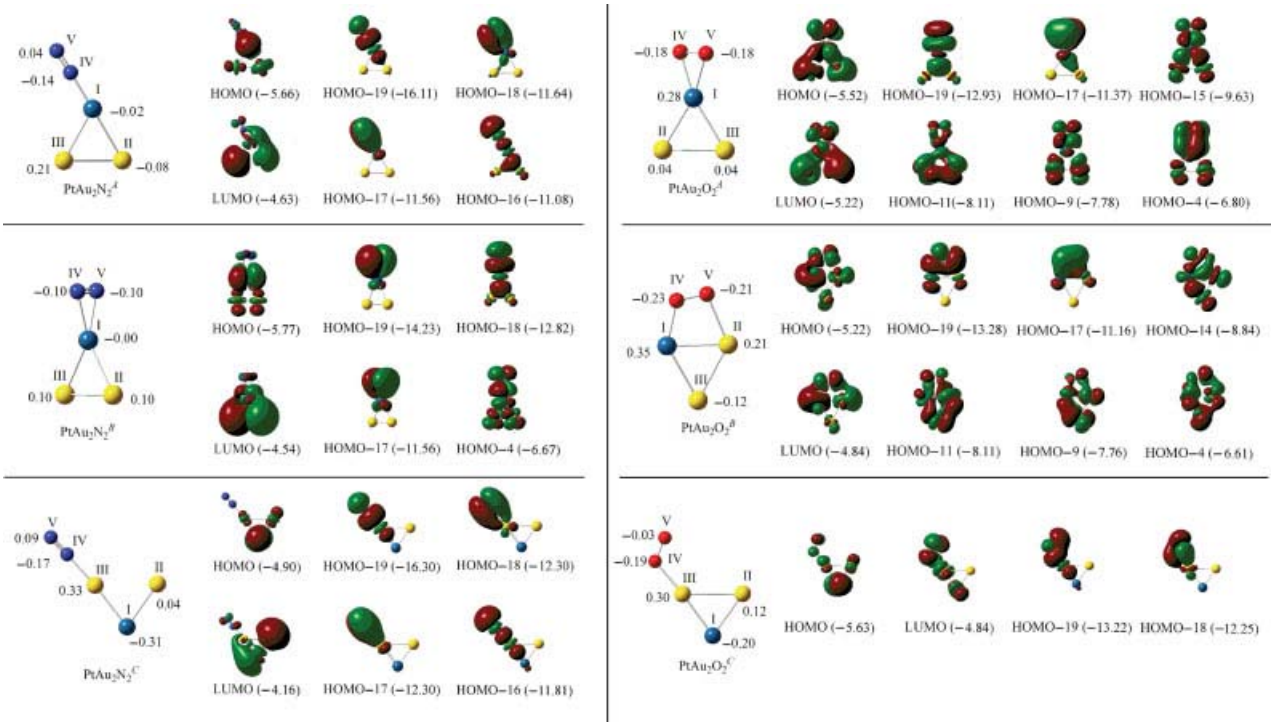

FIGURE 6. Molecular orbitals relevant to the bonding interactions between the diatomic fragment and the $PtAu_2$ fragments in the $PtAu_2N_2$ and $PtAu_2O_2$ adducts. HOMO–p denotes the p*th* orbital below the HOMO. Orbital energies (in eV) are shown in the parentheses. Partial charges are marked beside atomic sites. [Color figure can be viewed in the online issue, which is available at wileyonlinelibrary.com.]

orbitals of N_2 with the 6s5d-type orbitals of Pt. A remarkable feature in $PtAu_2N_2^{A,C}$ is that the binding strength varies greatly according to different binding sites. For example, the HOMO of the ground state of $PtAu_2$ is localized on the Pt atom and leads to a stronger N_2–Pt interaction than any other interaction between N_2 and a Au atom. The situation of N_2 binding to pure Au clusters is very similar to the case of N_2 binding to the Au atoms in the bimetallic clusters and hence will not be discussed further.

The $PtAu_2N_2^B$ complex has a different set of bonding orbitals from those of the above two complexes, $PtAu_2N_2^{A,C}$. The HOMO-19, a σ-type bonding orbital, is composed of the 5d orbital of Pt and the σ^* orbital of N_2. The two perpendicular π orbitals of N_2 play different roles here. In the HOMO-18 of $PtAu_2N_2^B$, one π orbital of N_2 overlaps with a d-type orbital of Pt to form a σ bond. The other π orbital of N_2 overlaps with another d-type orbital of Pt to form a π bond, the HOMO-17. The higher-lying HOMO-4 is composed of a π^* orbital of N_2 and a d orbital of Pt.

Partial charges are labeled on the corresponding atoms in Figure 6. Overall, the 2p orbitals of N_2 withdraw about 0.2 electrons from the metal clusters in the N_2–cluster complexes. Electrons migrate toward the N_2 fragment primarily from the direct bonding atoms in the clusters: Pt at site I in both $PtAu_2N_2^{A,B}$ and Au at site III in $PtAu_2N_2^C$. Also, about 0.1–0.2 electrons are promoted from 5d to 6s on the Pt atom on the adsorption of N_2.

Spin densities of open-shell structures were also examined by analyzing the $PtAu_3N_2$ complexes (Fig. 7). It was found that the majority of spin densities stays on the Pt atom in the cluster upon the N_2 adsorption. This indicates that any reaction with radicals will still occur toward the Pt atom of the cluster fragment.

In the N_2–cluster complexes, the HOMO still mainly localizes on the Pt site but to a less extent compared with the HOMO of the $PtAu_2$ cluster. This signifies that the HOMO energy of the N_2–cluster complexes resembles that of the $PtAu_2$ cluster and the Pt site is vulnerable to electrophilic attack. On the other hand, binding one N_2 molecule to the cluster changes the angular distribution and the extent of the localization of the HOMO on the Pt atom compared with the HOMO of $PtAu_2$. The HOMO of $PtAu_2N_2^A$ consists of 10% 6s, 58% $5d_{z^2}$, 3% $5d_{x^2-y^2}$,

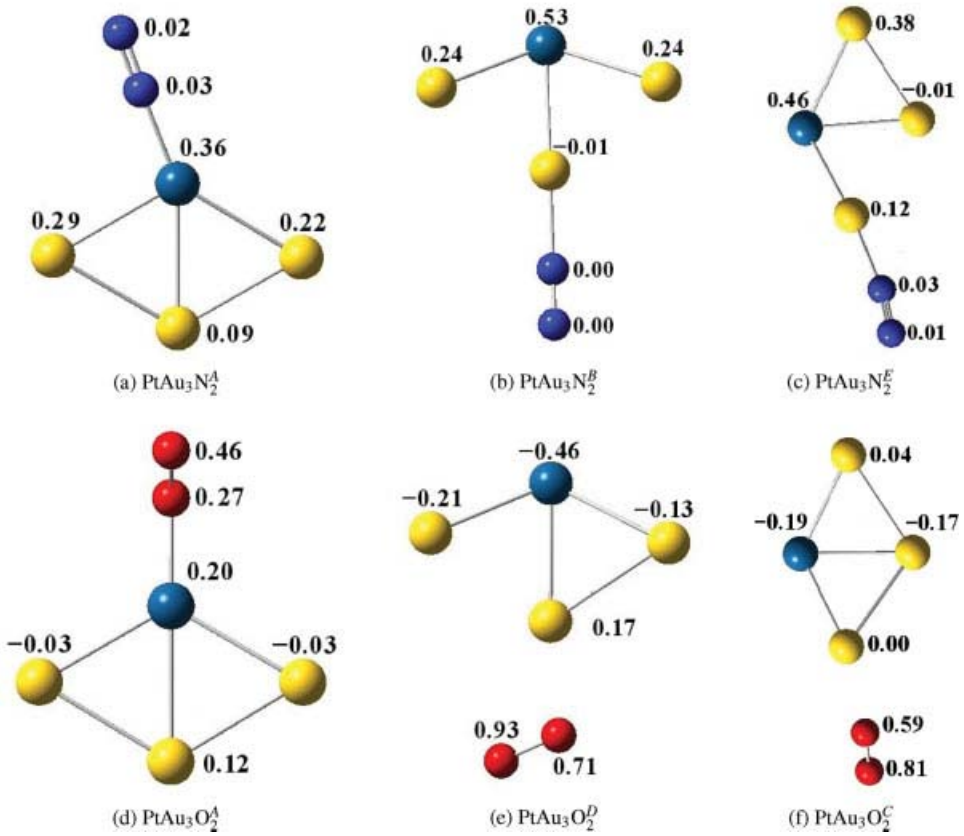

FIGURE 7. Natural spin densities of the atoms in the open-shell N_2/O_2–cluster complexes. The Pt, Au, N, and O atoms are in dark green, yellow, blue, and red, respectively. [Color figure can be viewed in the online issue, which is available at wileyonlinelibrary.com.]

and 8% of $5d_{xy}$ of the Pt atom, 3% 5d and 18% 6s of the Au atoms (Fig. 6). The HOMO of $PtAu_2N_2^B$ is composed of 62% $5d_{z^2}$, 15% $5d_{x^2-y^2}$, and 2% $5d_{z^2}$ of the Pt atom, 5% 5d contributions from the two Au atoms (Fig. 6). The cluster fragments in these two complexes, in which N_2 binds directly to the Pt atom, extend their HOMOs to the two Au atoms. In $PtAu_2N_2^C$, the HOMO stays strongly localized on the Pt atom and has 4% 6s and 72% $5d_{z^2}$ from the Pt atom and 3% 5d orbitals from the two Au atoms. Compared with the $PtAu_2$ cluster, the localization of the HOMO on the Pt atom remains for the $PtAu_2N_2^C$ complex but to a less extent than in the two most stable complexes ($PtAu_2N_2^{A,B}$). The orientation of the HOMO is markedly different, because of the change in the angular composition of the HOMO on the adsorption of N_2 onto the cluster.

In contrast to the preferred end-on adsorption pattern in forming the N_2–cluster complexes, O_2 tends to assume a side-on approach to the clusters. Bonding orbitals of the three different O_2–$PtAu_2$ complexes, $PtAu_2O_2^{A,B,C}$, are drawn in Figure 6. In the $PtAu_2O_2^A$ complex, the π or π^* orbital of O_2 and the d-type orbitals of the Pt atom contribute mostly to the bonding interaction between O_2 and the metal cluster in the complexes. Particularly, the two π bonding orbitals of O_2 overlap with the 5d orbitals of Pt to form a σ bond (HOMO-19) and a π bond (HOMO-17). In addition, the π^* orbital of O_2 participates in the formation of three σ bonds (HOMO-15, HOMO-11, and HOMO-9) and a π bond (HOMO-4). It is very difficult to analyze bonding interactions in $PtAu_2O_2^B$ through well-defined O_2 and metal cluster molecular orbitals. Nevertheless, the relevant orbitals are composed of the π and π^* orbitals of O_2 and the 5d orbitals from the Pt atom and the involved Au atom. Bonding patterns between O_2 and the Au atom in the bimetallic clusters resemble those between O_2 and the pure Au clusters. Thus, the O_2–Au_m complexes are not discussed further.

Partial charge analysis indicates that O_2 withdraws more electrons (0.2–0.6 electrons) from the

metal clusters than N_2 does in the N_2–cluster complexes. In $PtAu_2O_2^A$, about 0.5 electrons from the 5d orbitals of Pt transfer to the 2p orbitals of the two O atoms. In $PtAu_2O_2^B$, both the Pt atom and the Au atom at site II donate electron, but in different ways: from 6s and 5d of the Pt atom to the 2p orbital of O at site III and from the 6s orbital of Au at site II to the O atom at site V. In $PtAu_2O_2^C$, the Au atom at site III depletes electrons from its 5d orbitals to the 2p orbitals of the O atom at site IV.

The distribution of spin densities in the spin-unsaturated O_2–cluster complexes is different from that in the N_2–cluster complexes (Fig. 7). In $PtAu_3O_2^{A,C}$, spin densities are on the O atom away from the metal cluster fragment. In $PtAu_3O_2^D$, the total spin density is mainly on the two O atoms. This spin density distribution in the O_2–adsorption complex prompts any further reactions with radicals toward the two O atoms.

The compositions of the HOMOs of the O_2–cluster complexes depend strongly on the O_2–cluster binding pattern. In the clusters where O_2 binds to the Pt atom ($PtAu_2O_2^{A,B}$), the HOMO is primarily composed of the p orbitals on the O atoms and the 5d orbitals on the Pt atom. This leads to a large variation in the HOMO energy compared with that of the $PtAu_2$ cluster. The O atoms are thus susceptible to electrophilic attack in these two complexes ($PtAu_2O_2^{A,B}$). The HOMO of $PtAu_2O_2^A$ is more delocalized to the entire complex and consists of 3% $5d_{xz}$, 3% $5d_{yz}$, 9% $5d_{x^2-y^2}$, and 5% $5d_{xy}$ on the Pt atom, 29% p_x, 7% p_y, and 6% p_z from the two O atoms, and 20% 6s and 8% 5d from the two Au atoms. In $PtAu_2O_2^B$, the HOMO is mainly located on the O atoms (29% p_z on two O atoms, 21% $5d_{xz}$, 14% $5d_{x^2-y^2}$, and 5% $5d_{xy}$ of the Pt atom) and makes the two O atoms the nucleophilic sites. In $PtAu_2O_2^C$, where O_2 binds to the Au atoms, the HOMO remains strongly localized on the Pt atom as in the $PtAu_2$ cluster and comes from 59% $5d_{z^2}$, 3% 6s, and 6% $5d_{xz}$ of the Pt atom, and 2% p_z of the two O atoms, and 2% $5d_{z^2}$ of the Au atoms. Further electrophilic attack will prefer the Pt site in $PtAu_2O_2^C$.

4. Conclusions

We have studied the electronic structures of both pure Au_m and bimetallic $PtAu_n$ clusters. Clusters larger than a dimer tend to form (near) two-dimensional structures with basic triangular units. Substitution of one Au atom by Pt in small clusters leads to localized HOMOs and enhanced regioselective electron donating abilities. In open-shell bimetallic clusters, the spin charge density is localized on the Pt atom, which behaves as the active center in reactions with radicals.

We have also studied the N_2–cluster and O_2–cluster adsorption complexes and found that adsorption onto the Pt site of the bimetallic clusters leads to higher binding energies than adsorption to the pure Au clusters and to the Au atoms of the same bimetallic clusters. In N_2–cluster adsorption complexes, clusters donate their electrons to the σ^* orbitals of N_2, resulting in an end-on adducting configuration. In O_2–cluster adsorption complexes, more complicated cluster–O_2 π orbital interactions favor a side-on approach. The HOMOs of the N_2–bimetallic cluster adsorption complexes remain localized on the Pt site, but with varied directionality, while the adsorption of O_2 onto the Pt site delocalizes the HOMO onto the O atoms. For open-shell species, the spin density stays on the cluster fragment in the N_2–cluster adsorption complexes, whereas in the O_2–cluster adsorption complexes, the spin density gathers around the O atoms instead.

References

1. Link, S.; Wang, Z. L.; El-Sayed, M. A. J Phys Chem B 1999, 103, 3529.
2. Zhang, H.; Zelmon, D. E.; Deng, L.; Liu, H. K.; Teo, B. K. J Am Chem Soc 2001, 123, 11300.
3. Gaudry, M.; Lermé, J.; Cottancin, E.; Pellarin, M.; Vialle, J. L.; Broyer, M.; Prével, B.; Treilleux, M.; Mélinon, P. Phys Rev B 2001, 64, 085407.
4. Stener, M.; Albert, K.; Rõsch, H. Inorg Chim Acta 1999, 286, 30.
5. Bromley, S. T.; Catlow, C. R. Int J Quantum Chem 2003, 91, 270.
6. Tada, H.; Suzuki, F.; Ito, S.; Akita, T.; Tanaka, K.; Kawahara, T.; Kobayashi, H. J Phys Chem B 2002, 106, 8714.
7. Adams, R. D.; Barnard, T. S. Organometallics 1998, 17, 2885.
8. Vicente, J.; Chicote, M. T.; Hvertas, S. Inorg Chem 2001, 40, 6193.
9. Pederson, M. Ø.; Helveg, S.; Ruban, A.; Stensgaard, I.; Lægsgaard, E.; Nørskov, J. K.; Besenbacher, F. Surf Sci 1999, 426, 395.
10. Chandler, B. D.; Pignolet, L. H. Catal Today 2001, 65, 39.
11. Koszinowski, K.; Schröder, D.; Schwarz, H. J Am Chem Soc 2003, 125, 3676.
12. Koszinowski, K.; Schröder, D.; Schwarz, H. Angew Chem Int Ed Engl 2004, 43, 121.
13. Koszinowski, K.; Schröder, D.; Schwarz, H. Chemphyschem 2003, 4, 1233.

14. Tian, W. Q.; Ge, M.; Gu, F.; Aoki, Y. J Phys Chem A 2005, 109, 9860.
15. Tian, W. Q.; Ge, M.; Gu, F.; Yamada, T.; Aoki, Y. J Phys Chem A 2006, 110, 6285.
16. Song, C.; Ge, Q.; Wang, L. J Phys Chem B 2005, 109, 22341.
17. Mills, G.; Gordon, M. S.; Metiu, H. J Chem Phys 2003, 118, 4198.
18. Olson, R. M.; Varganov, S.; Gordon, M. S.; Metiu, H.; Chretien, S.; Piecuch, P.; Kowalski, K.; Kucharski, S. A.; Musial, M. J Am Chem Soc 2005, 127, 1049.
19. Häkkinen, H.; Moseler, M.; Landman, U. Phys Rev Lett 2002, 89, 033401.
20. Tian, W. Q.; Ge, M.; Sahu, B. R.; Wang, D.; Yamada, T.; Mashiko, S. J Phys Chem A 2004, 108, 3806.
21. Dai, D.; Balasubramanian, K. J Chem Phys 1995, 103, 648.
22. Fortunelli, A. J Mol Struct: Theochem 1999, 493, 233.
23. Berces, A.; Hackett, D. A.; Lian, L.; Mitchell, S. A.; Rayner, D. M. J Chem Phys 1998, 108, 5476.
24. Mihut, C.; Descorme, C.; Duprez, D.; Amiridis, M. D. J Catal 2002, 212, 125.
25. Amiridis, M. D.; Mihut, C.; Jaciejewski, M.; Baiker, A. Top Catal 2004, 28, 141.
26. Shi, Z. PEM Fuel Cell Electrocatalysis and Catalyst Layers; Springer, 2008; Chapter 5.
27. Knickelbein, M. B. Annu Rev Phys Chem 1999, 50, 79.
28. Perdew, J. P.; Burke, K.; Ernzerhof, M. Phys Rev Lett 1996, 77, 3865.
29. Frisch, M. J.; Trucks, G. W.; Schlegel, H. B.; Scuseria, G. E.; Robb, M. A.; Cheeseman, J. R.; Montgomery, A. J., Jr.; Vreven, T.; Kudin, K. N.; Burant, J. C.; Millam, J. M.; Iyengar, S. S.; Tomasi, J.; Barone, V.; Mennucci, B.; Cossi, M.; Scalmani, G.; Rega, N.; Petersson, G. A.; Nakatsuji, H.; Hada, M.; Ehara, M.; Toyota, K.; Fukuda, R.; Hasegawa, J.; Ishida, M.; Nakajima, T.; Honda, Y.; Kitao, O.; Nakai, H.; Klene, M.; Li, X.; Knox, J. E.; Hratchian, H. P.; Cross, J. B.; Bakken, V.; Adamo, C.; Jaramillo, J.; Gomperts, R.; Stratmann, R. E.; Yazyev, O.; Austin, A. J.; Cammi, R.; Pomelli, C.; Ochterski, J. W.; Ayala, P. Y.; Morokuma, K.; Voth, G. A.; Salvador, P.; Dannenberg, J. J.; Zakrzewski, V. G.; Dapprich, S.; Daniels, A. D.; Strain, M. C.; Farkas, O.; Malick, D. K.; Rabuck, A. D.; Raghavachari, K.; Foresman, J. B.; Ortiz, J. V.; Cui, Q.; Baboul, A. G.; Clifford, S.; Cioslowski, J.; Stefanov, B. B.; Liu, G.; Liashenko, A.; Piskorz, P.; Komaromi, I.; Martin, R. L.; Fox, D. J.; Keith, T.; Al-Laham, M. A.; Peng, C. Y.; Nanayakkara, A.; Challacombe, M.; Gill, P. M. W.; Johnson, B.; Chen, W.; Wong, M. W.; Gonzalez, C.; Pople, J. A. Gaussian 03; Gaussian, Inc.: Wallingford, CT, 2004.
30. Hay, P. J.; Wadt, W. R. J Chem Phys 1999, 82, 299.
31. Martin, J. M. L.; Bauschlicher, C. W.; Ricca, A. Comput Phys Comm 2001, 133, 189.
32. Reed, A. E.; Curtiss, L. A.; Weinhold, F. Chem Rev 1988, 88, 899.
33. Morse, M. D. Chem Rev 1986, 86, 1049.
34. James, A. M.; Kowdczyk, P.; Simard, B.; Pinegar, J. C.; Morse, M. D. J Mol Spectrosc 1994, 168, 248.
35. Dai, D.; Balasubramanian, K. J Chem Phys 1994, 100, 4401.
36. BonačićKoutecký, V.; Burda, J.; Mitrić, R.; Ge, M.; Zampella, G.; Fantucci, P. J Chem Phys 2002, 117, 3120.